MODELING OF MIXING OF SECONDARY AIR WITH GAS-SOLID SUSPENSION IN CFB RISERS

Murat Koksal, Feridun Hamdullahpur
Dalhousie University-DalTech, Department of Mechanical Engineering
B3J 2X4, Halifax, Nova Scotia, Canada
mkoksal@is2.dal.ca, fhamdull@is.dal.ca

INTRODUCTION

Circulating fluidized bed (CFB) technology has been successfully utilized in many industrial processes such as fossil fuel combustion, coal gasification and fluid catalytic cracking (FCC) due to its superior characteristics over low velocity (bubbling and turbulent) fluidized beds. The cited advantages of CFB reactors over low velocity fluidized bed reactors can be listed as improved gas-solid contacting, higher slip velocity between gas and particles, reduced cross-sectional area for the same superficial gas velocity and good turndown capability [1,2].

In most applications of CFB reactors, the reactants are injected laterally at a certain height along the riser for different purposes [3]. For instance, in fossil fuel combustion, secondary air injection, apart from the primary fluidization air injected from the bottom of the bed, is an effective way of controlling NO_x formation [4]. Mixing of secondary air (SA) stream with the rising gas-solid suspension is an important aspect that needs to be considered in designing a CFB boiler. The estimated penetration length of SA jets are used to determine the width of the boiler cross-section [5]. Previous studies have shown that the lateral dispersion of gas, which is due to gas turbulence, is usually poor [6,7]. Leckner proposed that a reasonably complete mixing from a point source in a commercial CFB riser can only be attained after an axial distance of 50 times the bed diameter [7]. The potential of incomplete mixing of SA with the fuel and the rising gas-solid suspension may lead to hydrocarbon emissions or reverse sulfation at oxygen lean zones as well as NO_x formation at oxygen rich zones of the riser [3].

Secondary air-to-total fluidization air flow ratio (SA/TA), height of the secondary air injection port from the distributor plate, design of the injector (i.e. diameter, orientation..etc) and the operational conditions are the main parameters that affect the mixing of SA with the gas-solid suspension [8,9]. Thus, information about the effects of these parameters and the operating conditions on SA mixing problem is essential in determining the performance of a CFB combustor.

In this article, mixing of SA with the gas-solid suspension in a lab scale CFB riser is investigated using an Eulerian-Eulerain (two-fluid) approach. Fluent V4.5, a commercial software, is used for grid generation and simulations.

HYDRODYNAMIC MODEL

In two-fluid approach, both gas and solid phases are treated as interpenetrating continua. Thus, each phase is characterized by its own mass, momentum and energy conservation equations closed by suitable closure laws. The following equations are derived by ensemble averaging the local instantaneous equations and the interactions between the phases for an isothermal, incompressible flow of gas and solid phases without mass transfer [10].

Conservation of mass for gas and solid phases:

$$\frac{\partial}{\partial t}\left(\alpha_g \rho_g\right)+\nabla.\left(\alpha_g \rho_g \vec{U}_g\right)=0 \qquad (1)$$

$$\frac{\partial}{\partial t}\left(\alpha_s \rho_s\right)+\nabla.\left(\alpha_s \rho_s \vec{U}_s\right)=0 \qquad (2)$$

where α is volume fraction, ρ is density and $\vec{U}$ is mean velocity of each phase while g and s denote the gas and solid phases, respectively.

Conservation of momentum for gas and solid phases:

$$\frac{\partial}{\partial t}\left(\alpha_g \rho_g \vec{U}_g\right)+\nabla.\left(\alpha_g \rho_g \vec{U}_g \vec{U}_g\right)=-\alpha_g \nabla p + \nabla.\left[\alpha_g\left(\overline{\overline{\tau_g}}+\overline{\overline{\tau_g^{Re}}}\right)\right]+\alpha_g \rho_g \vec{g}+\beta\left(\vec{U}_g-\vec{U}_s\right) \qquad (3)$$

$$\frac{\partial}{\partial t}\left(\alpha_s \rho_s \vec{U}_s\right)+\nabla.\left(\alpha_s \rho_s \vec{U}_s \vec{U}_s\right)=-\alpha_s \nabla p-\nabla p_s + \nabla.\left[\alpha_s \overline{\overline{\tau_s}}\right]+\alpha_s \rho_s \vec{g}+\beta\left(\vec{U}_s-\vec{U}_g\right) \qquad (4)$$

where p is hydrostatic pressure shared by both phases, p_s is solid pressure, $\overline{\overline{\tau_g}}$ is gas laminar stress tensor, $\overline{\overline{\tau_g^{Re}}}$ gas turbulent or "Reynolds stress" tensor, $\overline{\overline{\tau_s}}$ is solid phase stress tensor and β is gas-solid momentum exchange coefficient. Both gas laminar and solid phase stress tensors can be expressed using a Newtonian stress-strain relation:

$$\overline{\overline{\tau_g}}=\mu_g\left[\nabla\vec{U}_g+\left(\nabla\vec{U}_g\right)^T\right] \qquad (5)$$

$$\overline{\overline{\tau_s}}=\left(\xi_s-\frac{2}{3}\mu_s\right)\nabla.\vec{U}_s\,\bar{\bar{I}}+\mu_s\left[\nabla\vec{U}_s+\left(\nabla\vec{U}_s\right)^T\right] \qquad (6)$$

where μ_g is gas absolute viscosity, μ_s is effective solid shear viscosity and ξ_s is solid bulk viscosity.

CLOSURE LAWS

Gas-Solid Momentum Exchange Coefficient, β:
Sylamlal and O'Brien proposed the following correlation for β [11]:

$$\beta = \frac{3}{4} C_d \frac{\alpha_g \alpha_s \rho_g}{V_{ts}^2 d_p} \left| \vec{U}_g - \vec{U}_s \right| \quad (7)$$

where d_p is particle diameter and V_{ts} is the ratio of terminal velocity of a group of particles to that of an isolated one given as:

$$V_{ts} = 0.5\left(K_1 - 0.06\,Re_p\right) + 0.5\sqrt{(0.06\,Re_p)^2 + 0.12\,Re_p(2K_2 - K_1) + K_1^2} \quad (8)$$

$$Re_p = \frac{\rho_g d_p \left| \vec{U}_g - \vec{U}_s \right|}{\mu_g} \quad (9)$$

$$C_d = \left(0.63 + \frac{4.8}{\sqrt{Re_p / V_{tg}}} \right)^2 \quad (10)$$

$K_1 = \alpha_g^{4.14}$ and

$$K_2 = 0.8\alpha_g^{1.28} \quad \text{if} \quad \alpha_g \le 0.85$$
$$K_2 = \alpha^{2.65} \quad \text{if} \quad \alpha_g > 0.85 \quad (11)$$

Solid phase pressure [12]:

$$p_s = \alpha_s \rho_s \Theta_s \left[1 + 2(1+e) g_o \alpha_s\right] \quad (12)$$

where e is particle-particle coefficient of restitution and g_o is radial distribution function given as [11]:

$$g_o = \frac{1}{1-\alpha_s} + \frac{3\alpha_s}{2(1-\alpha_s)^2} \quad (13)$$

The granular or pseudo temperature, Θ_s [m^2/s^2] describes the fluctuating energy of the solid phase as:

$$\frac{3}{2}\Theta_s = \frac{1}{2}\left\langle \vec{u}_s' . \vec{u}_s' \right\rangle \quad (14)$$

where $\langle\ \rangle$ denotes the ensemble averaging and $\vec{u}'$ is fluctuating component of solid phase velocity.

Solid phase bulk viscosity [11, 12]:

$$\xi_s = \frac{4}{3}\alpha_s \rho_s d_p g_o (1+e)\sqrt{\frac{\Theta_s}{\pi}} \quad (15)$$

Collisional part of the solid shear viscosity [11, 12]:

$$\mu_{s,coll} = \frac{4}{5}\alpha_s \rho_s d_p g_o (1+e)\sqrt{\frac{\Theta_s}{\pi}} \quad (16)$$

Kinetic part of the solid shear viscosity [11]:

$$\mu_{s,kin} = \frac{d_p \rho_s \sqrt{\Theta_s \pi}}{6(3-e)}\left[1 + \frac{2}{5}(1+e)(3e-1)\alpha_s g_o\right] \quad (17)$$

The granular temperature is found by solving the solid fluctuating energy balance equation [12]:

$$\frac{3}{2}\left[\frac{\partial}{\partial t}(\alpha_s \rho_s \Theta_s) + \nabla.(\alpha_s \rho_s \vec{U}_s \Theta_s)\right] = \left(-p_s \bar{\bar{I}} + \overline{\overline{\tau_s}}\right) : \nabla \vec{U}_s + \nabla.(k_\Theta \nabla \Theta_s) - \gamma_\Theta + \phi_{gs} \quad (18)$$

where k_Θ is the diffusion coefficient given as [11]:

$$k_\Theta = \frac{15 d_p \rho_s \alpha_s \sqrt{\Theta\pi}}{4(41-33\eta)}\left[1 + \frac{12}{5}\eta^2(4\eta-3)\alpha_s g_o + \frac{16}{15\pi}(41-33\eta)\eta\alpha_s g_o\right] \quad (19)$$

with $\eta = \frac{1}{2}(1+e)$ (20)

Dissipation of fluctuating energy [13]:

$$\gamma_\Theta = \frac{12(1-e^2) g_o}{d_p \sqrt{\pi}} \rho_s \alpha_s^2 \Theta^{3/2} \quad (21)$$

Energy exchange between gas and solid phases [12]:

$$\phi_{gs} = -3\beta\Theta \quad (20)$$

Gas Phase Turbulence
Gas phase turbulence is taken into account with a modified k-ε eddy viscosity model [14,15]. According to Boussinesq hypothesis:

$$\overline{\overline{\tau_g^{Re}}} = \left[-\frac{2}{3}\rho_g k_g - \frac{2}{3}\mu_{g,t}\nabla.\vec{U}_g\right]\bar{\bar{I}} + \mu_{g,t}\left[\nabla\vec{U}_g + \left(\nabla\vec{U}_g\right)^T\right] \quad (21)$$

where k_g [m^2/s^2] is the gas turbulent kinetic energy defined as:

$$k_g = \frac{1}{2}\left\langle \vec{u}_g' . \vec{u}_g' \right\rangle \quad (22)$$

and $\mu_{g,t}$ is the gas turbulent viscosity described as:

$$\mu_{g,t} = \rho_g C_{\mu,g} \frac{k_g^2}{\varepsilon_g} \quad (23)$$

where ε_g [m^2/s^3] is the dissipation rate of gas turbulent kinetic energy.
Gas turbulent kinetic energy and its dissipation rate are obtained from the solutions of two transport equations, (24) and (25):

$$\frac{\partial}{\partial t}(\alpha_g \rho_g k_g) + \nabla.(\alpha_g \rho_g \vec{U}_g k_g) = \alpha_g\left(\overline{\overline{\tau_g^{Re}}} : \nabla\vec{U}_g\right) + \nabla.\left(\alpha_g \frac{\mu_{g,t}}{\sigma_{k,g}}\nabla k_g\right) - \alpha_g \rho_g \varepsilon_g + \Pi_{k,g}$$

$$\frac{\partial}{\partial t}(\alpha_g \rho_g \varepsilon_g) + \nabla.(\alpha_g \rho_g \vec{U}_g \varepsilon_g) = \alpha_g \frac{\varepsilon_g}{k_g}\left[C_{1\varepsilon,g}\left(\overline{\overline{\tau_g^{Re}}} : \nabla\vec{U}_g\right) - \rho_g C_{2\varepsilon,g}\varepsilon_g\right] + \nabla.\left(\alpha_g \frac{\mu_{g,t}}{\sigma_{\varepsilon,g}}\nabla\varepsilon_g\right) + \Pi_{\varepsilon,g}$$

where $\Pi_{k,g}$ and $\Pi_{\varepsilon,g}$ are the terms which represent the effects of the solid phase on gas phase kinetic energy and dissipation.

$$\Pi_{k,g} = \beta\alpha_g\rho_g\left(k_{gs} - 2k_g + \vec{U}_{dr}.\vec{U}_{rel}\right) \quad (26)$$

$$\Pi_{\varepsilon,g} = C_{\varepsilon 3,g}\frac{\varepsilon_g}{k_g}\Pi_{k,g} \text{ from [17]} \quad (27)$$

$$\vec{U}_{rel} = \left|\vec{U}_g - \vec{U}_s\right| \quad (28)$$

In the above equations, k_{gs} is the gas-particle covariance representing the correlation between the velocity fluctuations of the gas and solid phase and $\vec{U}_{dr}$ is the drift velocity describing the dispersion of particles by large scale turbulence [14]. A model for drift velocity was proposed by Deutsch and Simonin [14] with the assumption that the particles are suspended in homogenous turbulence as :

$$\vec{U}_{dr} = D_{gs}^t\left(\frac{1}{\alpha_g}\nabla\alpha_g - \frac{1}{\alpha_s}\nabla\alpha_s\right) \quad (29)$$

where D_{gs}^t is binary turbulent diffusion coefficient:

$$D_{gs}^t = \frac{1}{3}k_{gs}\tau_{gs}^t \quad (30)$$

τ_{gs}^t is eddy-particle interaction time or fluid Lagrangian integral time scale as viewed by particles:

$$\tau_{gs}^t = \tau_{g,E}\left(1 + C_\beta\varsigma^2\right)^{-1/2} \quad (31)$$

where $\tau_{g,E}$ is Eulerian integral time scale of gas phase given as:

$$\tau_{g,E} = \frac{3}{2}C_\mu\frac{k_g}{\varepsilon_g} \quad (32)$$

$$C_\beta = 1.8 - 1.35\cos^2\theta \quad (33)$$

θ is the angle between mean particle velocity and the mean relative velocity (28) and

$$\varsigma^2 = \frac{3\vec{U}_{rel}^2}{2k_g} \quad (34)$$

Gas-particle covariance, k_{gs}, is expressed as [14]:

$$k_{gs} = 2k_g\left(\frac{b + \eta_r}{1 + \eta_r}\right) \quad (35)$$

where η_r is the ratio of the Lagrangian integral time scale and particle relaxation time:

$$\eta_r = \frac{\tau_{gs}^t}{\tau_p} \quad (36)$$

Particle relaxation time is defined as:

$$\tau_p = \alpha_s\rho_s\beta^{-1}\left(\frac{\rho_s}{\rho_g} + C_v\right) \quad (37)$$

C_v is added mass coefficient taken as 0.5. Also from [14];

$$b = (1 + C_v)\left(\frac{\rho_s}{\rho_g} + C_v\right)^{-1} \quad (39)$$

The constants used in the model are the same as those of a single phase standard k-ε model except the $C_{\varepsilon 3,g}$ proposed by [17].

Table 1. Values of the constants used in the k-ε model for the gas phase.

$C_{\mu,g}$	$\sigma_{k,g}$	$\sigma_{\varepsilon,g}$	$C_{\varepsilon 1,g}$	$C_{\varepsilon 2,g}$	$C_{\varepsilon 3,g}$
0.09	1.0	1.3	1.44	1.92	1.2

Solid Phase Turbulence

Turbulent kinetic energy and viscosity of the solid phase are predicted in the framework of Tchen's theory [14,15,16]. Thus, solid phase turbulent kinetic energy and viscosity are expressed as:

$$k_s = k_g\left(\frac{b^2 + \eta_r}{1 + \eta_r}\right) \quad (40)$$

$$\mu_{s,t} = \rho_s\left[D_{gs}^t + \left(\frac{2}{3}k_s - b\frac{1}{3}k_{gs}\right)\tau_p\right] \quad (41)$$

Effective solid shear viscosity, μ_s, is the sum of the collisional and kinetic terms from kinetic theory and solid turbulent viscosity.

Interphase Turbulent Momentum Transfer [14]:

Interphase turbulent momentum transfer is taken into account by the following term added to the momentum exchange term in (3) and (4):

$$I_t = \beta\vec{U}_{dr} \quad (42)$$

Hence, for turbulent flows, the momentum exchange term in (3) and (4) is modified as:

$$\beta\left(\vec{U}_g - \vec{U}_s + \vec{U}_{dr}\right) \quad (43)$$

NUMERICAL SCHEME AND BOUNDARY CONDITIONS

Fluent V4.5 uses a control volume technique proposed by Patankar [19] to solve the system of conservation equations described. In this technique, the domain is divided into discrete control volumes using a general curvilinear grid and the governing equations are integrated over the individual control volumes to construct the algebraic equations solved by Line Gauss Siedel method for the discrete unknowns. The power-law differencing scheme is used for interpolation between grid points and to calculate the derivatives of the flow variables [19].

In all of the simulations performed in this study, the coefficient of restitution was taken to be 1. Hence,

particle collisions are assumed to be perfectly elastic. No slip boundary condition was applied for gas phase velocity whereas the solid phase was allowed to slip on the walls. The flux of the fluctuating kinetic energy of solid phase was set to be equal to zero at the wall. The inlet value of the granular temperature was taken to be same as the inlet velocity of the solid phase. At the near-wall region, standard wall function approach [20] was used for gas phase turbulence assuming that this approach does not cease to be valid for dilute gas-solid flows.

PREDICTION OF RISER FLOW IN A CFB

The described model was first tested against the results of the experiments performed by [18] in a lab scale CFB riser (0.075 m ID, 6.6 m high) with FCC particles (ρ_s =1714 kg/m^3, d_p = 75 μm). The simulations wre performed on a 2D Cartesian grid (105×35) for 30 s (Figure 1). Uniform, plug flow was assumed for both phases at the inlet. The superficial gas velocity and solids mass flux were set to be 2.89 m/s and 12 kg/m^2.s, respectively; same as the experimental values. The inlet volume fraction of FCC was set as 0.1, similar to experimental measurements. The inlet FCC velocity was determined from prescribed solids mass flux and volume fraction.

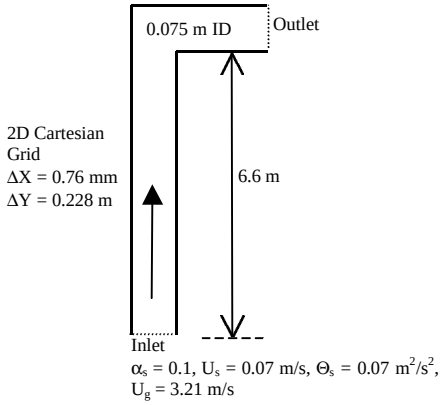

Figure 1. Simulation of IIT Riser [18].

Figures 2 and 3 compare the predicted FCC axial velocity and volume fraction with the experimental measurements at a height of 5.52 m from the distributor plate. Both figures show that the agreement with the experiments is reasonably good. Qualitatively, the model predicts the segregation near the wall region, typical to vertical gas-solid pipe flows, satisfactorily.

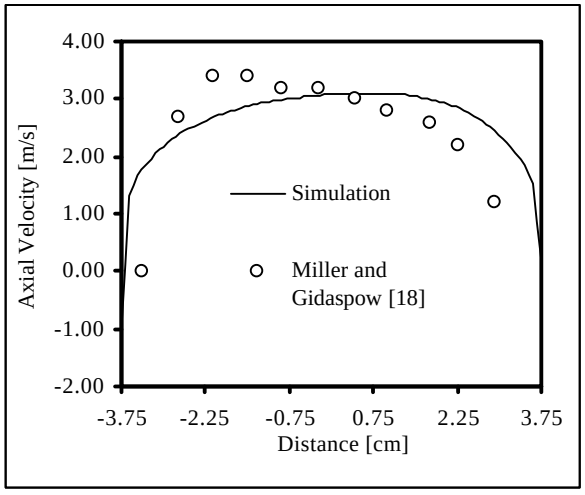

Figure 2. Comparison of FCC axial velocity prediction with the experiment.

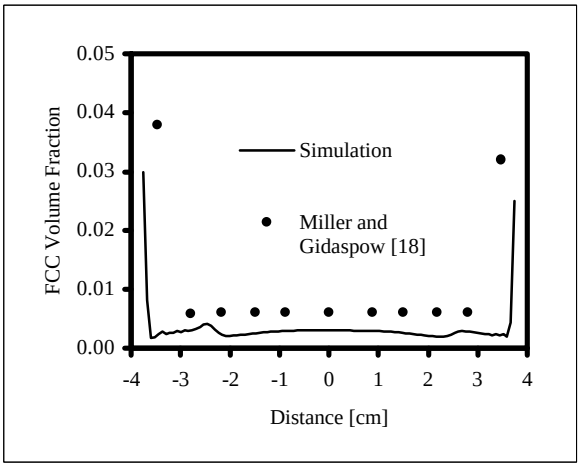

Figure 3. Comparison of FCC volume fraction prediction with the experiment.

APPLICATION OF MODEL TO SECONDARY AIR MIXING PROBLEM

The model is used to investigate the effects of solids loading and secondary-to-total air flow ratio (SA/TA) on the mixing behavior of SA with the gas-solid suspension. The geometry (Figure 4) of the grid was designed according to the dimensions of CFB pilot plant at Dalhousie University (7.6 m high, 0.23 m ID). The simulations were performed on a 2D Cartesian grid (50×40) for 10 seconds with sand particles ((ρ_s =2650 kg/m^3, d_p = 130 μm). The superficial gas velocity was kept constant at 5 m/s. Two different solid mass flux and SA/TA values were simulated; G_s = 10 kg/m^{2}s and 50 kg/m^{2}s, SA/TA = 0.25 and SA/TA = 0.5. Uniform, plug flow was assumed for both phases at the inlet with sand volume fraction being 0.02. The turbulent intensity of the air at both inlets were set as 5 %. Carbon dioxide, CO_2, was used as a tracer gas and mixed with SA. The

flow rate of CO_2 was set to be 1 % of the total flow rate in the simulations.

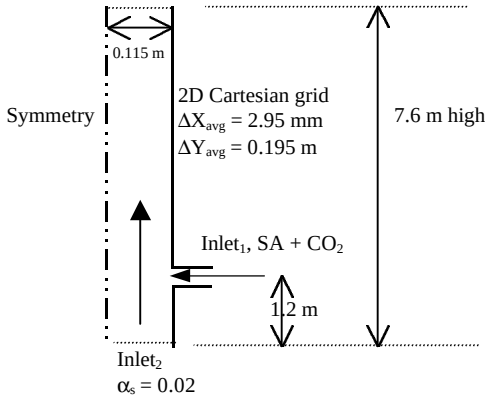

Figure 4. Grid geometry for SA mixing study

The transport of the tracer gas, CO_2, is governed by the following convection-diffusion equation:

$$\frac{\partial}{\partial t}\left(\rho_g Y_i\right)+\nabla.\left(\rho_g \vec{U}_g Y_i\right)=\nabla.\left(\Gamma_{eff}\nabla Y_i\right) \qquad (44)$$

where Y_i is the mass fraction of the tracer gas and Γ_{eff} is the effective dispersion coefficient of CO_2 in air given by:

$$\Gamma_{eff} = \rho_g D_{CO_2} + \frac{\mu_{g,t}}{Sc_t} \qquad (45)$$

D_{CO2} is the binary molecular diffusion coefficient of CO_2 in air (1.65×10^{-5} m^2/s at STP) and Sc_t is turbulent Schmidt number defined as:

$$Sc_t = \frac{\mu_{g,t}}{\rho_g D_t} \qquad (46)$$

D_t is the turbulent dispersion coefficient of CO_2 in air. A constant Schmidt number of 0.7 was used in the simulations.

The tracer concentration in the following figures was non-dimensionalized by dividing it by the mean mixed concentration, C_o, which is defined as the total tracer volumetric flow rate divided by the total fluidization air flow rate.

Figure 5 shows the prediction of tracer gas concentration at different elevations above SA injection port for solids mass flux, G = 10 kg/m^2s and SA/TA = 0.5. It is clearly seen that for the given conditions the mixing of SA with the rising gas-solid suspension is far from being satisfactory even at a height of 3 m above SA injection port.

Figures 6, and 7 show the effects of solids loading on mixing of SA with gas-solid suspension for SA/TA = 0.5 at two different elevations above the SA injection port. As can be inferred from these figures, mixing is retarded as the loading increases in the range of solids mass flux investigated. Thus, the quickest mixing along the riser is achieved in the case empty pipe.

Figure 8 presents the effects of SA/TA on mixing for G = 10 kg/m^2s. The trends of the curves are consistent with the fact that increasing SA/TA increases the mixing quality. As momentum of the SA increases with increasing SA/TA, the gas can penetrate more through the gas-solid suspension in the lateral direction increasing mixing. Also, the shear induced by the SA jet generates turbulence increasing its kinetic energy which in turn increases the net turbulent dispersion of gas in the lateral direction as shown in Figure 9. The gas phase turbulent kinetic energy for SA injection case is predicted an order of magnitude larger than that for non-SA injection case just above SA injection port as can be seen in Figure 9.

In the present formulation of mixing (44), (45) and (46), the dispersion coefficient is solely dependent on the gas turbulent viscosity, hence on gas phase turbulent kinetic energy. Thus, modeling of gas turbulence is the key element in predicting SA mixing. In gas turbulent kinetic energy equation (24), $\Pi_{g,k}$ represents "the energy necessary to accelerate the particles or the energy transferred from the particles to the gas phase if the particles have high fluctuation velocities in a region where the gas phase turbulent kinetic energy is low" [10]. In the range of operational conditions in current study with sand particles, the interaction term always acts to decrease the gas phase turbulent kinetic energy as shown in Figure 10. In fact, the results presented here are in agreement with the recent studies on turbulence modulation in two-phase flows [21, 22]. For instance, Hestroni [21] proposed that in a gas-solid flow, if $Re_p <$ 400, the gas phase turbulence is attenuated whereas it is augmented for $Re_p >$ 400. However, the degree of attenuation in gas phase turbulence is questionable and must be validated against experimental data. Especially, the effects of the constants used in k-ε model need more investigation as it was previously shown that they could be functions of Stokes number and solids loading [23]. Furthermore, the present formulation does not take the turbulence production in the wakes behind the particles which can also decrease the level of attenuation.

The future works is directed towards 3-D simulations and experimental validation of the results.

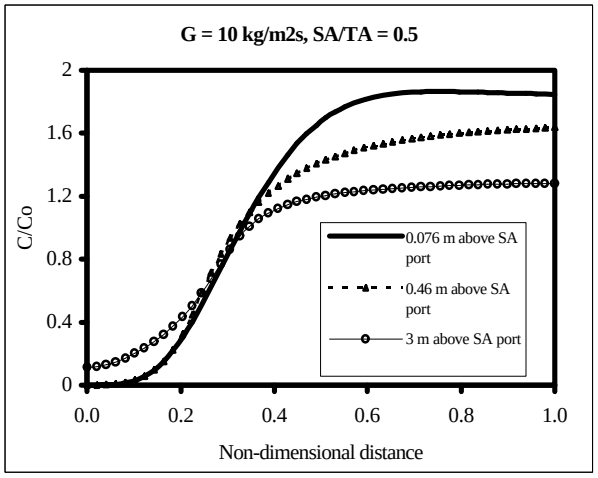

Figure 5. Non-dimensional tracer concentration for G= 10 kg/m^{2}s, SA/TA = 0.5

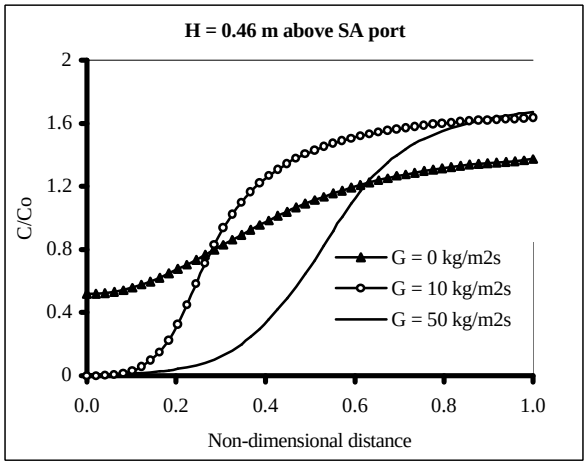

Figure 6. Non-dimensional tracer concentration for SA/TA = 0.5 (0.46 m above SA port)

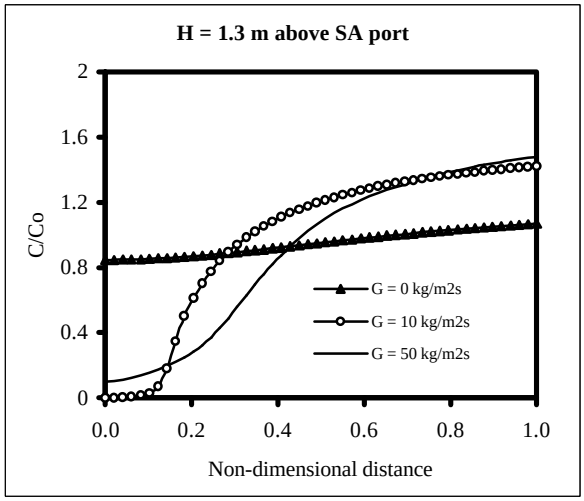

Figure 7. Non-dimensional tracer concentration for SA/TA = 0.5 (1.3 m above SA port)

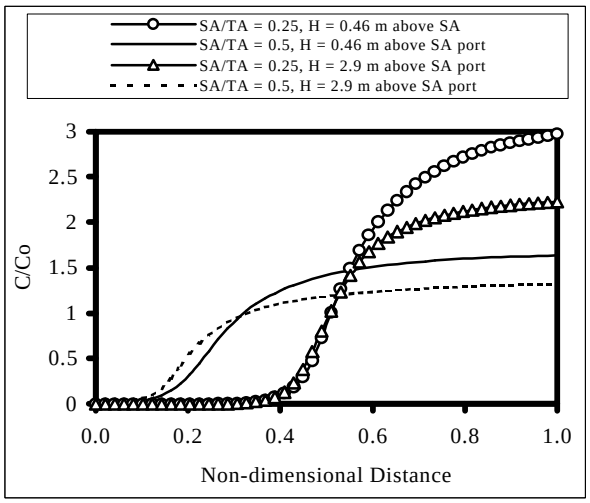

Figure 8. Effect of SA/TA on mixing (G = 10 kg/m^{2}s)

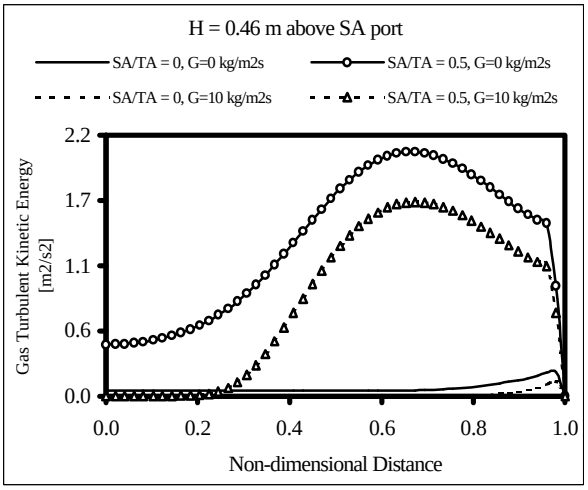

Figure 9. Effect of SA injection on gas phase turbulent kinetic energy.

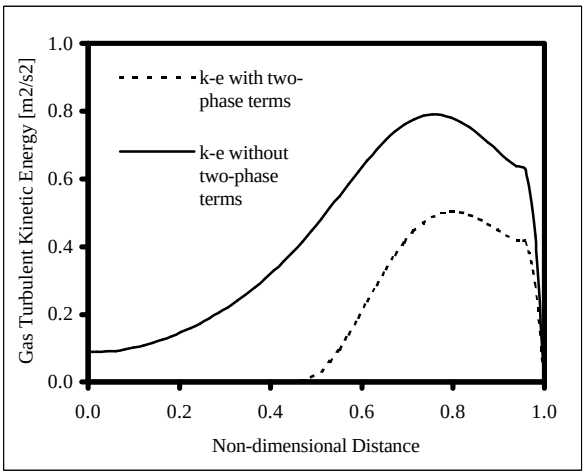

Figure 10. Effect of two-phase terms ($\Pi_{k,g}$ and ($\Pi_{\varepsilon,g}$) on gas phase turbulent kinetic energy (G = 10 kg/m^{2}s, SA/TA = 0.25, H = 0.46 m above SA port)

ACKNOWLEDGMENTS

The authors would like to thank Fluent Inc. for providing Fluent V4.5 under educational license agreement.

REFERENCES

1. Berruti, F., Chaouki, J., Pugsley, T.S., Patience, G.S., "Hydrodynamics of Circulating Fluidized Bed Risers: A Review", Canadian Journal of Chemical Engineering, vol. 73, p. 579-602, 1995.
2. Grace, J.R., Bi, H., "Fundamentals of Circulating Fluidized Beds", in Circulating Fluidized Beds, eds., Grace, J.R., Avidan, A.A., Knowlton, T.M., chp. 1, Chapman & Hall, London, 1997.
3. Arena, U., "Gas Mixing" in Circulating Fluidized Beds, eds., Grace, J.R., Avidan, A.A., Knowlton, T.M., chp. 3, pp. 86-118, Chapman & Hall, London, 1997.
4. Brereton, C., "Combustion Performance" in Circulating Fluidized Beds, eds., Grace, J.R., Avidan, A.A., Knowlton, T.M., chp. 10, pp. 369-416, Chapman & Hall, London, 1997.
5. Basu, P., Fraser, S.A., Circulating Fluidized Bed Boiler, Design and Operation, Butterworths-Heinemann-Reed Publishing Inc., Stoneham, MA., p. 182, 1991.
6. Couturier, M., Doucette, B., Stevens, D., Poolpol, S., Razbin, V.,"Temperature, Gas Concentration and Solid Mass Flux Profiles Within a Large Circulating Fluidized Bed Combustor", in Proceedings of 11th Int. Conference on Fluidized Bed Combustion, vol. 1, pp. 107-114, 1991.
7. Leckner, B., "Fluidized Bed Combustion: Mixing and Pollutant Limitation", Progress in Energy and Combustion Science, vol. 24, pp. 31-61, 1998.
8. Ersoy, L.E., "Effect of Secondary Air Injection on the Hydrodynamics of CFBs", PhD Thesis, Dalhousie University, 1998.
9. Marzocchella, A., Arena, U., " Hydrodynamics of a Circulating Fluidized Bed Operated with Different Secondary Air Injection Devices", Powder Technology, vol. 87, p. 185-191, 1996.
10. Enwald, H., Peirano, E., Almstedt, A.E., "Eulerian Two-Phase Flow Theory Applied to Fluidization", Int. J. Multiphase Flow, vol. 22, Suppl., p. 21-66, 1996.
11. Syamlal, M., Rogers, W., O'Brian, T.J., "MFIX Documentation, Theory Guide", technical note DOE/METC-94/10004, 1993.
12. Ding, J., Gidaspow, D., "A Bubbling Fluidization Model Using Kinetic Theory of Granular Flow", AIChE J, vol. 36, no. 4, p. 523-538, 1990.
13. Lun, C.K.K., Savage, S.B., Jeffrey, D.J., Chepurniy, N., "Kinetic Theories for Granular Flow:Inelastic Particles in Couette Flow and Slightly Inelastic Particles in a General Flow-Field", J. Fluid Mechanics, vol. 140, p. 223-256, 1984
14. Simonin, O., Viollet, P.L., "Prediction of an Oxygen Droplet Pulverization in a Compressible Subsonic Coflowing Hydrogen Flow", ASME FED, vol. 91, pp. 65-82, 1990.
15. F'dhila, B.R., Simonin, O., "Eulerian Prediction of a Turbulent Bubbly Flow Downstream of a Sudden Pipe Expansion", Proc. 5th Workshop on Two-phase Flow Predictions, Erlangen, Germany, pp. 1264-273, 1990.
16. Deutsch, E., Simonin, O., "Large Eddy Simulation Applied to the Motion of Particles in Stationary Homogeneous Turbulence", Turbulence Modification in Multiphase Flows, ASME FED, vol. 110, pp. 34-42, 1991.
17. Elgobashi, S.E., Abou-Arab, T.W., "A Two-Equation Turbulence Model for Two-Phase Flows", Physics of Fluids, vol. 26(4), p. 931-938, 1983.
18. Miller, A., Gidaspow, D., "Dense, Vertical Gas-Solid Flow in a Pipe", AIChE J., vol., 38(11), pp. 1801-1815, 1992.
19. Patankar, S.V., Numerical Heat Transfer and Fluid Flow, Hemisphere, New York, 1980.
20. Launder, B.E., Spalding, D.B., "The Numerical Computation of Turbulent Flows", Computer Methods in Applied Mechanics and Engineering, vol. 3., pp. 269-289, 1974.
21. Hestroni, G., "Particles-Turbulence Interaction", Int. J. Multiphase Flow, vol. 15, No. 5, pp. 735-746, 1989.
22. Gore, R.A., Crowe, C.T., "Effect of Particle Size on Modulating Turbulent Intensity", Int. J. Multiphase Flow, vol. 15, no. 2, p. 279-285, 1989.
23. Squire, K.D., Eaton, J.K., "Effect of Selective Modification of Turbulence on Two-equation Models for Particle Laden Turbulent Flows", ASME J. Fluids Engineering, vol. 116, pp. 778-784, 1994.